Lithium–Oxygen Batteries Hot Paper

DOI: 10.1002/ange.201408008

Liquid-Free Lithium–Oxygen Batteries**

*Moran Balaish, Emanuel Peled, Diana Golodnitsky, and Yair Ein-Eli**

Abstract: *Non-aqueous lithium–oxygen batteries are considered as most advanced power sources, albeit they are facing numerous challenges concerning almost each cell component. Herein, we diverge from the conventional and traditional liquid-based non-aqueous Li–O_2 batteries to a Li–O_2 system based on a solid polymer electrolyte (SPE-) and operated at a temperature higher than the melting point of the polymer electrolyte, where useful and most applicable conductivity values are easily achieved. The proposed SPE-based Li-O_2 cell is compared to Li–O_2 cells based on ethylene glycol dimethyl ether (glyme) through potentiodynamic and galvanostatic studies, showing a higher cell discharge voltage by 80 mV and most significantly, a charge voltage lower by 400 mV. The solid-state battery demonstrated a comparable discharge-specific capacity to glyme-based Li–O_2 cells when discharged at the same current density. The results shown here demonstrate that the safer PEO-based Li–O_2 battery is highly advantageous and can potentially replace the contingent of liquid-based cells upon further investigation.*

Rechargeable Li–O_2 batteries based on non-aqueous electrolytes attracted much attention in recent years due to their outstanding theoretical energy density of about 3500 W h kg^{-1}.[1–4] However, there are some critical challenges regarding the electrolyte, hindering the actualization of a Li–O_2 battery as a high-energy storage device: 1) Most common organic liquid electrolytes are volatile and hence, are less suited for the Li–O_2 battery, which is in essence an open system. 2) The Achilles heel of most organic electrolytes is their long-term stability as they are prone to autoxidation under oxygenated radicals (formed during cell operation), being converted into unstable peroxide species.[5–11] 3) Low surface tension between the carbon surface of the air cathode and most organic electrolytes results in flooding of the air electrode and hence, only dissolved[11] O_2 participates in the actual oxygen reduction reaction (ORR) and the associated charge-transfer reaction, occurring in the two-phase boundary reaction zone.[12]

One approach to tackle all of the above problems is to design a liquid-free Li–O_2 cell which is safer and is based on a solid polymer electrolyte (Scheme 1). Polymers are expected to exhibit higher chemical, thermal, and electrochemical stabilities (see Figure S1 in the Supporting Information). Moreover, not only that the polymer can ensure safe cell operation, but it would also minimize oxygen crossover towards the anode and would totally eliminate the use of a separator in the cell. Despite the advantages pointed out, SPE has high internal resistance at room temperature, resulting from a low ionic mobility, high degree of polymer matrix crystallinity, and low degree of charge separation in addition to ion association, preventing their practical use as electrolyte in Li–O_2 batteries, unless inorganic fillers such as ZrO_2, Al_2O_3, SiO_2, TiO_2, and/or anion traps are used.[13–16] In 2011, Scrosati et al. used a ZrO_2-added PEO-based polymer composite electrolyte in a Li–O_2 battery, but when discharged at constant load, the battery failed to reach current densities higher than 20 μA cm^{-2}.[17]

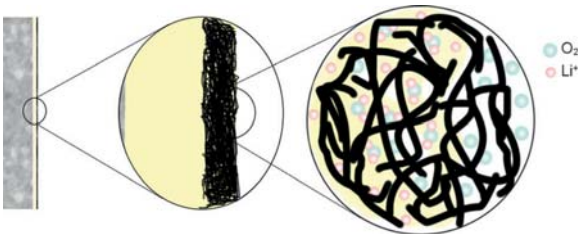

Scheme 1. Schematic representation of Li–O_2 battery comprised of lithium anode (gray), $P(EO)_{20}LiTf$ electrolyte (yellow), and CNT air-cathode (black).

Herein, we deviate from the conventional Li–O_2 battery operated at room temperature to a polymer-based Li–O_2 system operated at a temperature higher than the melting point of the poly(ethylene oxide)–lithium triflate electrolyte ($T_m = 70.55$ °C according to differential scanning calorimetry, DSC, analysis; Figure S2), where it predominantly exists in the amorphous state. This, in turn, results in practical and useful conductivity values of the solid electrolyte. To minimize thermal oxidation of poly(ethylene oxide) at high temperatures,[18–23] the operating temperature of the SPE-based Li–O_2 cell was determined to be 80 °C, thus achieving acceptable ionic conductivity, comparable to common organic

[*] Prof. Y. Ein-Eli
Department of Materials Science and Engineering and
The Nancy & Stephen Grand Technion Energy Program
Technion-Israel Institute of Technology
Haifa, 3200003 (Israel)
E-mail: eineli@tx.technion.ac.il
M. Balaish
The Nancy & Stephen Grand Technion Energy Program
Technion-Israel Institute of Technology
Haifa, 3200003 (Israel)
Prof. E. Peled, Prof. D. Golodnitsky
School of Chemistry, Tel Aviv University
Tel Aviv 69978 (Israel)

[**] The authors acknowledge the support from the Grand Technion Energy Program (GTEP), Israel National Research for Electrochemical Propulsion (INREP), the Helmsley Charity Fund and the Israeli Ministry of Energy and Water Resources.CNT fabrics were kindly provided and supplied by TorTech nano-fibers Ltd. (Koren Industrial Park, Maalot-Tarshicha, Israel).

Supporting information for this article is available on the WWW under http://dx.doi.org/10.1002/anie.201408008.

electrolytes in Li–O_2 systems (Figure S3) and lower overall cell impedance (Figure S4). In addition, the SPE Li–O_2 battery operated at 80 °C will tackle one of the main challenges of lithium-metal dendrite formation upon cycling.

Potentiodynamic polarization studies of the lithium metal/Pt couple (anodic half-cell) and CNT/Pt (oxygen) electrode couple (cathodic half-cell) with 1 M LiTf/triethylene glycol dimethyl ether (triglyme) and $P(EO)_{20}$LiTf (P(EO) = poly(-ethylene oxide) and LiTf = lithium triflate) were conducted to determine whether the latter could serve as electrolyte in the Li–O_2 battery with a reasonable battery performance (Figure 1). While conducting the polarization close to open circuit potential (OCP), the potential difference between the

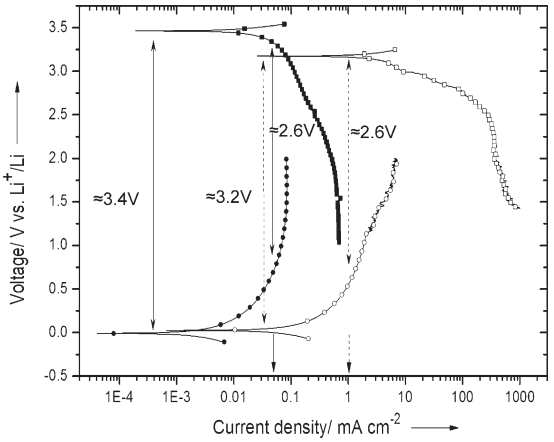

Figure 1. Potentiodynamic polarization plot obtained in $(PEO)_{20}$LiTf electrolyte (bold black) and 1 M LiTf/triglyme (black) at a scan rate of 20 mV s^{-1} from air electrode (rectangular) and lithium metal (circle) at 80 °C and room temperature, respectively.

cathodic and anodic curves was 3.4 V, compared to an OCP of 3.2 V for the 1 M LiTf/triglyme-based cell operated at room temperature. This difference can be assigned to a temperature difference, as well as to different lithium ion and oxygen chemical potentials. Surprisingly, it is evident from Figure 1 that the lithium metal is the limiting component in both the polymer- and liquid-based electrolyte systems, as the air cathode promotes one to two orders of magnitude higher current densities, respectively. Saying that, we recognize that in a full Li–O_2 cell additional factors need to be well considered; for example, under long cell operational conditions, deposition of insulating discharge products (lithium peroxide) lowers the cathode effective active area for reaction, as well as blocking paths for oxygen transportation, all in all leading to higher over-potential, turning the cathode to the real limiting component (see Figure S5 for further information). The anodic polarization plot of the SPE-based cell could have implied poorer lithium dissolution/deposition performance. However, when a symmetric Li/$P(EO)_{20}$LiTf/Li cell was subjected to galvanostatic polarization (0.1 mA cm^{-2}) at 80 °C, an over-potential of only 20 mV for lithium striping and plating was observed (Figure S6). In addition, Figure S7 presents the potential distributions of the air cathode and Li anode in a three-electrode cell, verifying that during discharge the potential of the Li anode remains constant at 30 mV versus Li^+/Li, while the air electrode contributes to most of the overall voltage drop of the Li–O_2 cell, maintaining it as the limiting component, dictating the rate capability of the Li–O_2 cell.

Both anodic and cathodic potentiodynamic plots conducted at high temperature indeed revealed much information, albeit further studies of the system at different current densities were required. Li–O_2 cells using $P(EO)_{20}$LiTf were constructed (see the Experimental Section and a movie in the Supporting Information). Simultaneously, a conventional Li–O_2 cell consisting of 1 M LiTf/triglyme electrolyte soaked in celgard® separator having all components of the cell being identical to the PEO-based cell was assembled and discharged at room temperature. The cells were discharged under dry oxygen (1 atm) to a potential of 2.2 V (Figure 2 a). In both cases, a free-standing (binder-free and metal-free) CNT fabric served as the air cathode (see the Experimental Section and Figure S8 for further information on the electronic contact and a movie in the Supporting Information). After discharging, the SPE-based Li–O_2 cell was disassembled and the CNT cathode was removed, washed with deuterated acetonitrile

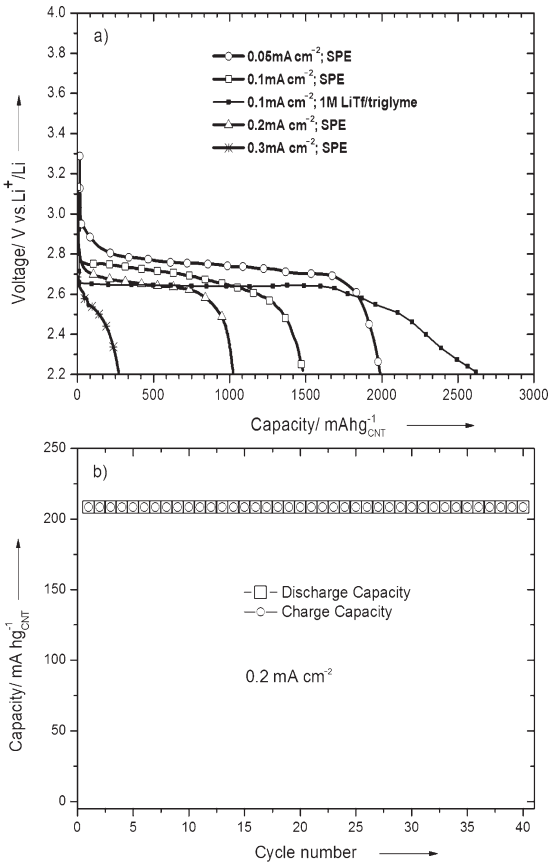

Figure 2. Discharge profiles of the Li–O_2 cell. a) Discharge curves of the SPE-based Li–O_2 cell at different current densities (0.05, 0.1, 0.2, 0.3 mA cm^{-2} in circle, rectangular, triangle and asterisk, respectively. In addition, discharge curve of 1 M LiTf/triglyme-based Li–O_2 cell is presented (0.1 mA cm^{-2} in bold rectangular); b) cycling stability of the SPE-based Li–O_2 cell at a current density of 0.2 mA cm^{-2}.

(for further NMR spectroscopy analysis) and examined by X-ray diffraction (XRD; Figure S9). The electrode exhibited peaks at 32.9°, 35°, 40.7°, and 58.8°, characteristics of pure crystalline Li_2O_2, as the main discharge product. The open circuit voltage of the polymeric cell was about 3.3 V, and the average discharge voltage of the cells varied between 2.5–2.7 V, depending on the discharge current density.[24] The lower ionic conductivity in $(PEO)_{20}$LiTf at 80 °C and higher interfacial resistance compared to the 1 M LiTf/triglyme liquid electrolyte at room temperature (approximately one order of magnitude smaller) cannot be excluded, but is roughly compensated by the lack of a separator, leading both cells to similar IR drop values (0.5 V). When both cells were discharged at a current density of 0.1 mA cm^{-2} the specific discharge capacity and average discharge voltage (calculated based on Ref. [24]) were 2620 mAh g_c^{-1}, 1481 mAh g_c^{-1} and 2.58 and 2.66 V, respectively. The cyclying stability of the polymeric cell at a current density of 0.2 mA cm^{-2} is displayed in Figure 2b (refer to Figure S10 for the discharge/charge profiles). Unlike the liquid-based cells, possessing a charging voltage of 4–4.2 V, the polymeric cell charging voltage was about 3.6 V, consistent with previously reported values indicating lower charging-over-potential for polymeric system in the solid state or in clusters compared to a liquid-based system.[17] Low Li^+ migration and diffusion, as well as low oxygen diffusion can naturally affect the overall cell performance, resulting in lower specific discharge capacity in the polymeric system, and ultimately leading to different discharge termination mechanism. SEM images of the pristine electrode and discharged CNT electrode are presented in Figure 3 (refer to Figure S11 for additional SEM images). To investigate the distribution of the deposited lithium peroxide on the CNT electrodes, the last was sectioned to different thicknesses of 10–20 μm and SEM images of the cathode were acquired from the side facing the polymer electrolyte (Figure 3c), at approximately 10 μm in depth (Figure 3d) and at 20 μm in depth (Figure 3e and f). While polymer residues are noticeable in Figure 3c, when penetrating deeper into the CNT air-cathode, the discharge products are revealed throughout the entire cathode thickness. The polymer electrolyte, being more viscous than room-temperature glymes, can actually forces the formation of a desirable three-phase reaction zones in the outer (air-facing) sections of the air electrode. By doing so, the deposition of lithium peroxide is enabled throughout most of the cathode volume, leading to higher capacities. However, the lower capacity of the polymeric cell (Figure 2) can further imply a different discharge termination mechanism. In the case of glyme-based electrolytes, the deposition of the insulating and insoluble lithium peroxide terminates the discharge process long before oxygen diffusion turns to be the rate-limiting step.[25] It is possible that in the polymeric cell, the viable limiting step is indeed the low oxygen diffusion, as supported by the potentiodynamic polarization plots presented earlier in Figure 1.

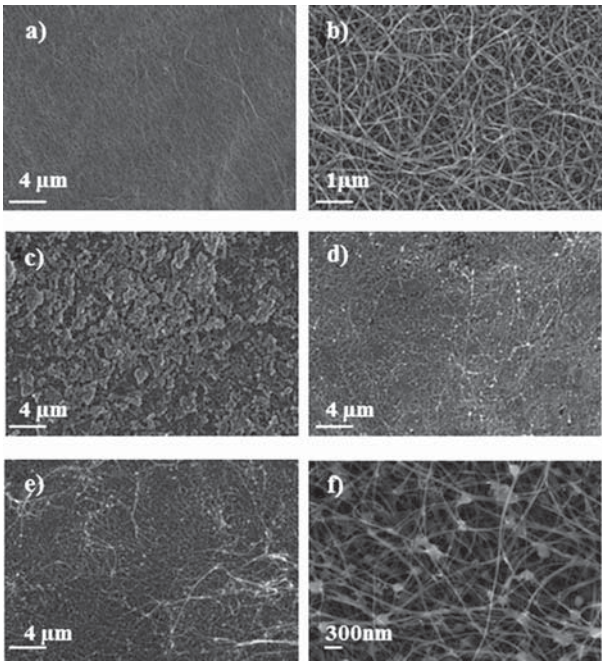

Figure 3. High-resolution SEM images of a,b) the pristine CNT air-cathode, c) the CNT air-cathode after discharged in a SPE-based Li–O_2 cell at 0.1 mA cm^{-2} to 2.2 V acquired at the side facing the polymer electrolyte, d) after pealing about 10 μm of the CNT cathode, and e,f) after pealing about 20 μm of the CNT cathode.

Study of SPE degradation was carried out using NMR spectroscopy. After discharging the polymeric cell at a current density of 0.05 mA cm^{-2} the air cathode was removed and soaked in deuterated acetonitrile for at least 24 h. ^{1}H and ^{13}C NMR spectra obtained for the original and degraded $P(EO)_{20}$LiTf are shown in Figure S12 and Figure 4, respectively. The ^{1}H spectrum of pristine polymer-salt complex presents an intense singlet at 3.59 ppm from interior main-chain OCH_2 protons and an additional singlet at 2.57 ppm from hydroxy end-groups, while the ^{13}C NMR spectrum showed a degraded $P(EO)_{20}$LiTf, as small new peaks appeared in the spectrum, as well as an intense peak at 71.08 ppm from main-chain OCH_2 carbon atoms. The small new peaks appeared in the spectrum are indicated with the following chemical shifts: a) 2.93 ppm, broad; b) 3.30 ppm, singlet; c) 3.57 ppm, singlet; d) 3.59-3.63, multiplet; e) 3.91 ppm, singlet; f) 4.68, group of singlets; g) 8.28 ppm, singlet. While peak (c) is well assigned to the main-chain OCH_2 protons, the peaks marked as (d) indicate the existence of lower-molecular-weight PEO macromolecules, produced by random chain scission of C–O bonds.[19] The ^{13}C NMR spectrum confirms this with the appearance of small singlets at 70.6, 70.8, 70.9, 71.1, 71.2, and 72.9 ppm, in addition to the intense singlet at 71.3 ppm from interior repeating units. Peak (b) together with a ^{13}C peak at 61.91 ppm can be assigned to the methoxy end-group, -OCH_3-. The minor ^{1}H degradation peak (f) can be assigned to the oxymethylene group, -OCH_2-O-, and correlates well with the minor ^{13}C peak at 95 ppm. Although this group of singlets seems at first glance to be a spin–spin coupling multiplet, its frequency span remains constant while running a spectrum at a frequency of 300 MHz. An additional minor ^{1}H degradation peak (g) may be assigned to the methanoate end-group, -O-CO-H. The absence of singlets in the range of 160–170 ppm in the

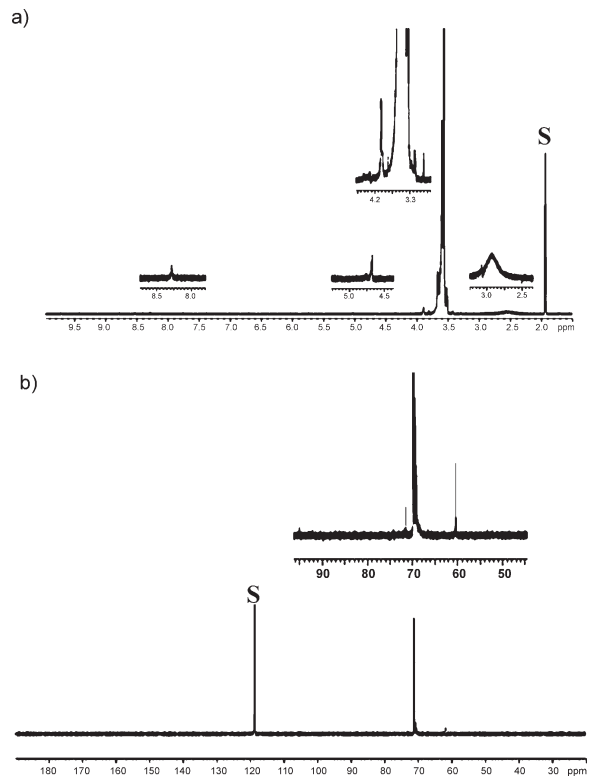

Figure 4. a) ^{1}H NMR spectrum of SPE after discharge at 0.05 mA cm^{-2} to 2.2 V at 80 °C. Expansion of the 2.5–3, 3.3–4.2, 4.5–5, 8–8.5 ppm regions are presented. b) ^{13}C NMR spectrum of SPE after discharge at 0.05 mA cm^{-2} to 2.2 V at 80 °C. Expansion of the 45–96 ppm region is presented. The peaks labelled by S indicates the solvent peak.

^{13}C NMR spectrum might be due to the following reasons: a small amount of products, T_1 values for the carbonyl carbon are 4 to 7 higher than those of main-chain CH_2 carbon atoms in the 60–70 ppm region,[20] and a low sensitivity of the ^{13}C nucleus compared to the ^{1}H nucleus. The broad singlet (peak a) correlates well with the presence of hydroxyl end-groups, as well as water as a side product, via the formation of formates and esters. Further studies of the electrolyte decomposition products during ORR, were conducted with the use of FT-IR analysis of the SPE subsequent to a storage at 80 °C in an oxygen environment. The FT-IR spectrum (Figure S13) shows two pronounced absorption peaks at 1177 cm^{-1} (C–O stretching), 1720 cm^{-1} (C=O stretching), attributed to the formation of formats and an additional absorption band at 1607 cm^{-1} (antisymmetrical stretching of the carboxylate ion). Another absorption band with a maximum at 1746 cm^{-1} (C=O stretching) can be attributed to the presence of an ester.[21,26] Combining the gained knowledge from both ^{1}H and FT-IR spectra lead us to assign peak (e) to the presence of esters, despite the lack of an appropriate peak in the ^{13}C NMR spectrum for the reasons explained above.

A proposed mechanism for the formation of various products is presented in Scheme 2. PEO is known to be sensitive towards thermal oxidation, occuring on the carbon atom in an α position to the oxygen atom (**1**),[21] followed by the formation of hydroperoxides (**2**) as primary products and theirs decomposition is followed by the formation of a macro-alkokoxy radicals (**3**) which can further react to produce esters by a cage reaction (**4**) and/or formates by β-scission (**5**) of the alkoxy radical. Repetition of the last reaction will eventually result in a considerable chain shortening, leading to lower-molecular-weight PEO chains.[18–20,23] Formates can further react, producing oxymethylene (**6**) and methoxy (**7**) as illustrated in Scheme 2. Although, the presence of lithium salt can reduce the strength of backbone C–O bonds leading to the formation of aldehydes (**8**),[18] no experimental evidence of this reaction path was observed, while the degradation products identified above were quantified from the ^{1}H NMR spectrum. It was found that a pulse interval of 71 seconds was sufficient to allow full relaxation of all peaks. Table S1 provides a detailed listing of the different functional groups identified as degradation products of the solid electrolyte and provides a quantitate figure of merit, relative to the amount of the remaining ethylene oxide units -OCH_2CH_2-. It is evident from Table S1 that although esters and formates were identified as possible degradation products, their amount

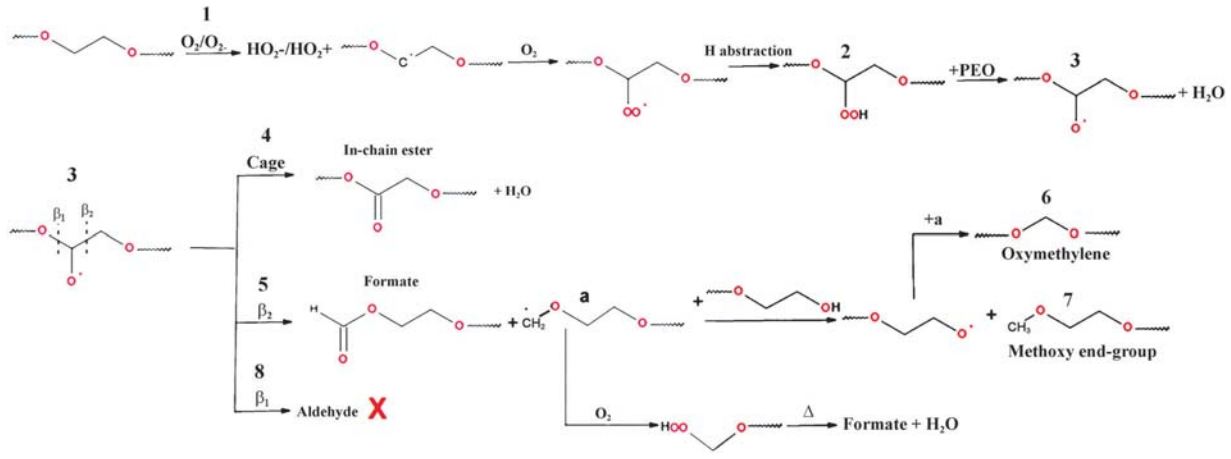

Scheme 2. Proposed mechanism for degraded P(EO)$_{20}$LiTf electrolyte after discharged in a Li–O_2 cell at 0.05 mA cm^{-2}.

was one and two orders of magnitude lower compared to PEO chains of different molecular weights, respectively.

In conclusion, we hereby presented an SPE-based Li–O_2 battery operated at 80 °C. By combining electrochemical studies with powder X-ray diffraction, FTIR, and NMR spectroscopy, it has been shown that PEO can serve as an electrolyte in Li–O_2 cell with minor electrolyte decomposition. The decomposition products consist of a mixture of lower-molecular-weight PEO, esters, formates, oxymethylene, methyl methanoate, and water, accompanied by the presence of lithium peroxide as a discharge product. Although the basic version of SPE-based Li–O_2 cell exhibited lower electrochemical and discharge performance compared to glyme-based Li–O_2 cell, the advantages of such a system rise well above its flaws. Higher discharge voltage as well as broad distribution of lithium peroxide throughout the bulk volume of the air cathode confirm the Li–O_2 SPE system as a highly advanced one that should be further studied and developed. The challenges of such a system can be resolved by either designing a binary and ternary electrolyte systems composed of a polymer–organic solvent–ionic liquid systems,[27,28] as well as a custom-made synthesis of PEO chains that can possibly lead to improved stability. This can be achieved by replacing some of the hydrogen atoms at the PEO chains with fluorine atoms. Inorganic fillers can also potentially improve the electrochemical stability of the polymer electrolyte by adsorbing contamination and side-reaction products. In addition, employing additives, which can increase oxygen concentration at the cathode active side,[29] can further improve the overall performance of the SPE-based Li-O_2 cell. While safety is a prime concern in Li-metal-based battery, it is of greater challenge once a viable Li–O_2 battery development is being considered. A polymer-based system, which is liquid electrolyte-free, seems to be another and important step towards resolving this issue.

Received: August 6, 2014
Revised: September 1, 2014
Published online: October 3, 2014

Keywords: carbon nanotubes · electrolytes · lithium–oxygen batteries · oxygen · polymers

[1] G. Girishkumar, B. McCloskey, A. Luntz, S. Swanson, W. Wilcke, *J. Phys. Chem. Lett.* **2010**, *1*, 2193 – 2203.
[2] J. Xiao, D. Mei, X. Li, W. Xu, D. Wang, G. L. Graff, W. D. Bennett, Z. Nie, L. V. Saraf, I. A. Aksay, *Nano Lett.* **2011**, *11*, 5071 – 5078.
[3] J. Zheng, R. Liang, M. Hendrickson, E. Plichta, *J. Electrochem. Soc.* **2008**, *155*, A432 – A437.
[4] T. Ogasawara, *J. Am. Chem. Soc.* **2006**, *128*, 1390.
[5] M. Balaish, *Phys. Chem. Chem. Phys.* **2014**, *16*, 2801.
[6] K. U. Schwenke, *Phys. Chem. Chem. Phys.* **2013**, *15*, 11830.
[7] D. Waddington, *Proc. R. Soc. London Ser. A* **1959**, *252*, 260 – 272.
[8] V. S. Bryantsev, *J. Phys. Colloid Chem.* **2012**, *116*, 7128.
[9] H. Wang, K. Xie, *Electrochim. Acta* **2012**, *64*, 29 – 34.
[10] D. Sharon, V. Etacheri, A. Garsuch, M. Afri, A. A. Frimer, D. Aurbach, *J. Phys. Chem. Lett.* **2013**, *4*, 127 – 131.
[11] S. A. Freunberger, *Angew. Chem. Int. Ed.* **2011**, *50*, 8609; *Angew. Chem.* **2011**, *123*, 8768.
[12] S. S. Zhang, D. Foster, J. Read, *J. Power Sources* **2010**, *195*, 1235 – 1240.
[13] H. Mazor, *Isr. J. Chem.* **2008**, *48*, 259.
[14] H. Mazor, D. Golodnitsky, E. Peled, W. Wieczorek, B. Scrosati, *J. Power Sources* **2008**, *178*, 736 – 743.
[15] M. Kalita, A. Plewa-Marczewska, G. Żukowska, E. Sasim, W. Wieczorek, M. Siekierski, *Electrochim. Acta* **2010**, *55*, 1298 – 1307.
[16] F. Croce, *Nature* **1998**, *394*, 456.
[17] J. Hassoun, F. Croce, M. Armand, B. Scrosati, *Angew. Chem. Int. Ed.* **2011**, *50*, 2999; *Angew. Chem.* **2011**, *123*, 3055.
[18] L. Costa, *Macromolecules* **1992**, *25*, 5512.
[19] O. A. Mkhatresh, F. Heatley, *Polym. Int.* **2004**, *53*, 1336 – 1342.
[20] O. A. Mkhatresh, F. Heatley, *Macromol. Chem. Phys.* **2002**, *203*, 2273 – 2280.
[21] S. Morlat, J. Gardette, *Polymer* **2001**, *42*, 6071 – 6079.
[22] L. Shibryaeva, *Thermal Oxidation of Polypropylene and Modified Polypropylene-Structure Effect*, INTECH, **2012**, pp. 63 – 86.
[23] L. Yang, F. Heatley, T. G. Blease, R. I. G. Thompson, *Eur. Polym. J.* **1996**, *32*, 535 – 547.
[24] M. Balaish, A. Kraytsberg, Y. Ein-Eli, *J. Electroanal. Chem.* **2013**, *707*, 85 – 88.
[25] V. Viswanathan, K. S. Thygesen, J. Hummelshøj, J. K. Nørskov, G. Girishkumar, B. McCloskey, A. Luntz, *J. Chem. Phys.* **2011**, *135*, 214704.
[26] C. Wilhelm, J. Gardette, *Polymer* **1998**, *39*, 5973 – 5980.
[27] S. Joon-Ho, W. A. Henderson, S. Passerini, *J. Electrochem. Soc.* **2005**, *152*, A978 – A983.
[28] S. Joon-Ho, W. A. Henderson, S. Passerini, *Electrochem. Commun.* **2003**, *5*, 1016 – 1020.
[29] M. Balaish, A. Kraytsberg, Y. Ein-Eli, *ChemElectroChem* **2014**, *1*, 90 – 94.

